IEEE Access
Multidisciplinary | Rapid Review | Open Access Journal

Received February 17, 2020, accepted March 2, 2020, date of publication March 9, 2020, date of current version March 18, 2020.

Digital Object Identifier 10.1109/ACCESS.2020.2979234

Adaptive Backstepping Sliding Mode Dynamic Positioning System for Pod Driven Unmanned Surface Vessel Based on Cerebellar Model Articulation Controller

ZAIJI PIAO[1], CHEN GUO[1], (Member, IEEE), AND SHUANG SUN[2]
[1]School of Marine Electrical Engineering, Dalian Maritime University, Dalian 116026, China
[2]School of Maritime Economics and Management, Dalian Maritime University, Dalian 116026, China

Corresponding author: Chen Guo (dmuguoc@126.com)

This work was supported in part by the National Natural Science Foundation of China under Grant 51879027, Grant 51579024, Grant 61374114, and Grant 51809028, and in part by the Fundamental Research Funds for the Central Universities under Grant DMU 3132019318.

ABSTRACT The dynamic positioning system is a system that ships rely on their own propulsion devices to maintain position and course. Pod propulsion was more and more installed in dynamic positioning unmanned surface vessels because it can rotate 360 degrees freely. The maximum disturbance of unmanned surface vessel dynamic positioning comes from the forces and moments generated by the ocean wind, wave and current. In order to improve its accuracy of disturbance rejection, the mathematical model of the vessel was established according to the special structure of pod propulsion ship, and the calculations of the forces and moments of wind, wave and current are given. Then, the sliding mode controller based on approach law and adaptive backstepping were designed, and optimal controller based on cerebellar model articulation controller (CMAC) was further designed. The tracking differentiator was added to eliminate the large chattering in the initial stage of the system. Finally, the simulation verification was carried out. It can be seen from the results that the control law designed has better control effects than traditional sliding mode control and can realize dynamic positioning of pod driven unmanned surface vessel under certain disturbances.

INDEX TERMS Cerebellar model articulation controller, dynamic positioning system, pod propulsion, sliding mode control, unmanned surface vessel.

I. INTRODUCTION

Unmanned surface vessel (USV) is a huge and complex system, which involves many theories and technologies, such as ship design and manufacture, sensor technology, intelligent decision-making, maritime communication [1], etc. USV is a kind of special mobile robot in essence, so its research can be carried out by the technology of mobile robot or rotorcraft flying robot [2], [3]. At present, many countries are competing to develop USV [4]. The United States Navy began to study the USV in the 1990s. In 2007, the United States Navy issued the Navy's master plan for USV, which gave it seven tasks, and defined the ship type, size and standard, which marked that the USV of United States embarked on the formal development stage. Israel's ''protector'' USV has begun mass production which already equipped by the military. Singapore Navy is its first overseas user. In one test, they used landing ships to carry two ''protector'' USV for maritime defense and blockade operations. According to Singapore's Ministry of Defense, ''protector'' is very efficient. Germany and Japan are also studying USV actively. The development of China's USV is still in its infancy, and progress has been made in civil use. Such as the ''tianxiang-1'' USV was used as meteorological emergency equipment to provide meteorological support services for the Olympic sailing competition in Qingdao. The research of the USV can be divided into two types: full drive propulsion and underactuated propulsion. The problem of dynamic positioning is full drive control [5], [6]. Dynamic positioning system is an important part of the control system of USV. International maritime organization defines dynamic positioning system (DPS) as automatic control for the position and course of a ship only depend on its own propulsion system [7], [8]. Pod propulsion is often used for dynamic positioning ships. The pod propulsion improves

The associate editor coordinating the review of this manuscript and approving it for publication was Huiping Li.

the hydrodynamic characteristics and maneuverability of the ship. It integrates the propulsion and steering mechanism through a rotatable motor. It does not set the rudder unit which can save the space of the ship and increase the flexibility of the ship construction.

The control algorithm is the core of the dynamic positioning system of USV. This paper adopts the sliding mode control (SMC) algorithm based on Cerebellar Model Articulation Controller. SMC is applicable for linear, nonlinear, continuous, discrete, deterministic and uncertain systems [9]. This control method allows the system state to slide along the sliding surface, which makes the system invariable under external disturbance [10]. In 1950s, Emelyanov proposed sliding mode control. In 1977, Utkin studied it deeply and formed a set of systematic theory [11]. Since 1980s, there have been different kinds of sliding mode control, such as SMC of discrete system, adaptive SMC and terminal SMC, etc. In recent years, there have been multiple improved sliding mode control algorithms, such as neural SMC, fuzzy SMC and integral SMC, etc. The algorithm studied in this paper is sliding mode controller based on adaptive backstepping which is optimized by CMAC. CMAC is proposed by Albus in a series of basic papers according to Eccles cerebellar space-time model [12]. The cerebellar model simulates a learning structure of human cerebellum. It is a local approximation neural network based on table query, and provides a multi-dimensional nonlinear mapping ability from input to output. It has one disadvantage, that is, the storage space of the weight coefficient of the neural network increases sharply with the increase of the input dimension of the cerebellar model. In order to solve this problem, Thompson and Kwon used a neighborhood sequential method [13], and the weight coefficient of each memory unit is adjusted only once during the whole learning period, which can solve the problem of possible conflict in learning. Eldracher *et al.* used adaptive coding technology [14], which can effectively improve the approximation ability of cerebellar model function. In this paper, the good approximation ability of CMAC is used to track the output of sliding mode controller and gradually replaces the original controller to work independently. Thus, some unstable factors are eliminated and the controller is optimized.

The main contributions of this article are summarized as follows:

(1) The mathematical models of pod driven unmanned surface vessels and ocean disturbances are established to enhance dynamic positioning simulation, and in order to realize dynamic positioning, a sliding mode control law based on approach law is designed.

(2) In order to solve the problem of long adjustment time of traditional sliding mode control based on approach law, adaptive backstepping sliding mode control law based on CMAC neural network optimization is designed. It greatly improves the control effect and shortens the adjustment time.

(3) In order to solve the very large oscillation in the initial stage of control, the tracking differentiator is added into the controller. In this way, the large-scale oscillation in the initial stage of the system is eliminated. This kind of oscillation is very disadvantageous in actual control, and the actuator cannot produce this kind of control state quickly.

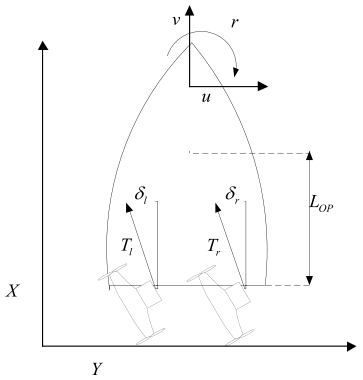

FIGURE 1. Layout diagram of pods.

The rest of this paper is organized as follows: Section 2 introduces the mathematical models of ship motion and ocean disturbances. Section 3 introduces the design method of the controller. Section 4 shows the results of simulation of dynamic positioning system.

II. MATHEMATICAL MODEL OF POD DRIVEN SHIP DYNAMIC POSITIONING SYSTEM

This paper discusses the motion of pod driven unmanned surface vessel with three degrees of freedom on the ocean [15]–[20]. Using pod propulsion can produce greater lateral force and gyroscopic moment than the rudder under the same turning angle.

Because the ships studied in this paper are symmetrically installed with two propeller pods, whose layout diagram is shown in Figure 1. The forces and moment produced by pods can be calculated as follows:

$$\begin{cases} X_P = 2(1-t_p)(T_l \cos\delta_l + T_r \cos\delta_r) \\ Y_P = 2(1-t_p)(T_l \sin\delta_l + T_r \sin\delta_r) \\ N_P = -Y_P L_{op} \\ T_{l/r} = \rho n_{l/r}^2 D_{l/r}^4 K_{l/r} \end{cases} \tag{1}$$

X_P, Y_P and N_P are the longitudinal force, transverse force and moment produced by pod; δ_l and δ_r are turning angles for left and right pod; L_{op} is half of the length of the ship (L); t_p is the thrust deduction coefficient; T_l is the thrust of left pod; T_r is the thrust of right pod; ρ is the density of sea water; $n_{l/r}$ is the speed of the propeller; $D_{l/r}$ is the diameter of the propeller; $K_{l/r}$ is the thrust calculation coefficient. Subscripts "l" and "r" mean left pod and right pod respectively.

Mathematical Model of Ship is:

$$M\dot{V} + DV = \tau_T + \tau_D \tag{2}$$

$V = [u, v, r]^T$ is ship velocity vector, which are longitudinal speed, transverse speed and steering moment. $\tau_T = [X_T, Y_T, N_T]^T$ means the longitudinal force, transverse force and moment of pods. $\tau_D = [X_D, Y_D, N_D]^T$ means the longitudinal force, transverse force and moment of disturbances,

inertia matrix

$$\mathrm{M} = \begin{bmatrix} m - X_{\dot{u}} & 0 & 0 \\ 0 & m - Y_{\dot{v}} & Y_{\dot{r}} \\ 0 & -N_{\dot{v}} & I_{zz} - N_{\dot{r}} \end{bmatrix}$$

and damping matrix

$$\mathrm{D} = \begin{bmatrix} -X_u & 0 & 0 \\ 0 & -Y_v & -Y_r \\ 0 & -N_v & -N_r \end{bmatrix}.$$

m is ship mass after dimensionless; I_{zz} is moment of inertia; $X_{\dot{u}}$, X_u, $Y_{\dot{v}}$, Y_v, $Y_{\dot{r}}$, $Y_r N_{\dot{v}}$, N_v $N_{\dot{r}}$, and N_r are hydrodynamic derivatives which can be obtained by sea trial and recursion [21].

The formulas of wind forces and moment are:

$$\begin{cases} X_{wind} = 0.5\rho_a U_R^2 A_f C_{wx} \\ Y_{wind} = 0.5\rho_a U_R^2 A_s C_{wy} \\ N_{wind} = 0.5\rho_a U_R^2 A_s L C_{wn} \end{cases} \tag{3}$$

Among the formulas, L is the length of ship; U_R is the relative wind velocity; ρ_a is the air density; A_s is the side of the projection area on the water line; A_f is the orthogonal projection area of the hull surface; C_{wx}, C_{wy} and C_{wz} can be calculated as (4):

$$\begin{cases} C_{wx} = X_0 + X_1 \cos\psi + X_3 \cos 3\psi + X_5 \cos 5\psi \\ C_{wy} = Y_1 \sin\psi + Y_3 \sin\ 3\psi + Y_5 \sin\ 5\psi \\ C_{wn} = N_1 \sin\psi + N_2 \sin\ 2\psi + N_3 \sin\ 3\psi \end{cases} \tag{4}$$

Among them, X_i, Y_i and N_i are obtained through a large number of ship wind tunnel tests [22].

In this paper, the formulas of wave forces and moment are:

$$\begin{cases} X_{wave} = \dfrac{1}{2}\rho g L \zeta_a^2 \cos\chi C_{Xw}^D(\lambda) \\ Y_{wave} = \dfrac{1}{2}\rho g L \zeta_a^2 \sin\chi C_{Yw}^D(\lambda) \\ N_{wave} = \dfrac{1}{2}\rho g L^2 \zeta_a^2 \sin\chi C_{Nw}^D(\lambda) \end{cases} \tag{5}$$

In this formula, ρ is sea water density; g is gravitational acceleration; ζ_a is the average wave amplitude; χ is the wave encounter angle; λ is the wavelength. C_{Xw}^D, C_{Yw}^D and C_{Nw}^D are coefficients summed up by ship model experiment, and the mathematical expressions are shown as (6). L is the ship length.

$$\begin{cases} C_{Xw}^D(\lambda) = 0.05 - 0.2(\dfrac{\lambda}{L}) + 0.75(\dfrac{\lambda}{L})^2 - 0.51(\dfrac{\lambda}{L})^3 \\ C_{Yw}^D(\lambda) = 0.46 + 6.83(\dfrac{\lambda}{L}) - 15.65(\dfrac{\lambda}{L})^2 + 8.44(\dfrac{\lambda}{L})^3 \\ C_{Nw}^D(\lambda) = -0.11 + 0.68(\dfrac{\lambda}{L}) - 0.79(\dfrac{\lambda}{L})^2 + 0.21(\dfrac{\lambda}{L})^3 \end{cases} \tag{6}$$

This paper assumes that current as uniform current. In attach coordinate system, the current longitudinal and transverse velocities are:

$$\begin{cases} u_c = V_c \cos(\psi_c - \psi) \\ v_c = V_c \sin(\psi_c - \psi) \end{cases} \tag{7}$$

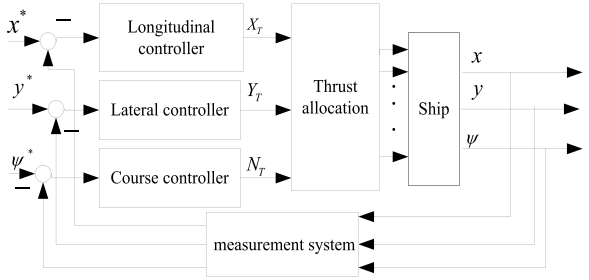

FIGURE 2. Control block diagram of DPS.

u_c and v_c are current longitudinal and transverse velocity; V_c is the current velocity relative to the earth; ψ_a is current angle; ψ is course angle.

$$\begin{cases} u_r = u - u_c \\ v_r = v - v_c \end{cases} \tag{8}$$

u_r and v_r are the ship longitudinal and transverse velocities; u and v are the velocity of the ship relative to the earth.Due to the assumption that current is under the condition of uniform flow, the ship's turning angular velocity r is consistent whether to the water or the ship. The derivative of (8) is obtained:

$$\begin{cases} \dot{u}_r = \dot{u} - r v_c \\ \dot{v}_r = \dot{v} + r u_c \end{cases} \tag{9}$$

III. DESIGN AND ANALYSIS OF CONTROLLER

The dynamic positioning system consists of the measurement system, control system and thrust allocation system [23]. During the voyage, the control system produces the control signals to resist the effects of various disturbances [24]. Control block diagram of DPS is shown in Figure 2. x^*, y^* and ψ^* are expected position and course; x, y and ψ are actual position and course; X_T, Y_T and N_T are the longitudinal force, transverse force and moment produced by controllers.

A. SLIDING MODE CONTROL ALGORITHM

Sliding mode control is a kind of special nonlinear control, whose nonlinear performance is the discontinuity of control. Its control principle is to design the switching hyperplane of the system according to the expected dynamic characteristics of the system, and to bind the system state from outside the hyperplane to the switching hyperplane. Once the system reaches the switching hyperplane, the control function will ensure the system along the switching hyperplane when the plane reaches the origin of the system. The advantage of sliding mode control is that it can overcome the uncertainty of the system and has strong robustness to the disturbance and unmodeled dynamics, especially for the nonlinear system. The disadvantage of this method is that when the state trajectory reaches the sliding mode surface, it is difficult to strictly follow the sliding mode towards the origin the balance point slides, but shuttles back and forth on both sides of the sliding surface, resulting in chattering.

The conventional sliding mode control law of dynamic positioning can be designed according to the following steps.

It is known from (2):

$$\dot{V} = -M^{-1}DV + M^{-1}(\tau_T + \tau_D) \tag{10}$$

$\eta = [x, y, \psi]^T$ are the longitudinal displacement, lateral displacement and heading angle of the ship.

$$\dot{\eta} = R(\psi)V \tag{11}$$

In (11),

$$R(\psi) = \begin{bmatrix} \cos\psi & -\sin\psi & 0 \\ \sin\psi & \cos\psi & 0 \\ 0 & 0 & 1 \end{bmatrix}.$$

So (12) can be deduced:

$$\begin{aligned} \ddot{\eta} &= R(\psi)\dot{V} + \dot{R}(\psi)V \\ &= -R(\psi)M^{-1}DR(\psi)^{-1}\dot{\eta} + R(\psi)M^{-1}\tau_T \\ &\quad + R(\psi)M^{-1}\tau_D + \dot{R}(\psi)V \end{aligned} \tag{12}$$

We set $\eta_d = [x_d, y_d, \psi_d]^T$, so the position error $e = \eta - \eta_d$. Then switching function is:

$$s_1 = \dot{e} + Ce \tag{13}$$

C is a diagonal matrix of 3×3, $C = \mathrm{diag}(c_1, c_2, c_3)$. So $\dot{s}_1 = \ddot{e} + C\dot{e}$, The design of controller based on the equal speed approach law:

$$\dot{s}_1 = -\varepsilon \mathrm{sgn}(s_1), \quad \varepsilon > 0 \tag{14}$$

So, the sliding mode control law is:

$$\begin{aligned} \tau_T = (R(\psi)M^{-1})^{-1}(C\dot{e} + \varepsilon \mathrm{sgn}(s_1) \\ + R(\psi)M^{-1}DR(\psi)^{-1}\dot{\eta} - R(\psi)M^{-1}\bar{\tau}_D) \end{aligned} \tag{15}$$

where $\bar{\tau}_D$ represents the upper bound of the total uncertainty τ_D. The Lyapunov method is used to determine the stability of the controller. The following Lyapunov function can be used:

$$V(x) = \frac{1}{2}s_1^2 \tag{16}$$

If $\dot{V}(x) < 0$, it is stable. The first derivative of the above function is $\dot{V}(x) = s_1\dot{s}_1$. So the following formula can be calculated:

$$\begin{cases} \because \varepsilon > 0 \\ \therefore \dot{V} = s_1\dot{s}_1 = -\varepsilon s_1 \mathrm{sgn}(s_1) < 0 \end{cases} \tag{17}$$

Therefore, the approach law can stabilize the system [25]–[28].

B. ADAPTIVE BACKSTEPPING SLIDING MODE CONTROLLER

The backstepping method is widely used in control system design. Because of the uncertainty of system parameters, (10) can be written as $\dot{V} = (-M^{-1}D + \Delta A)V + (M^{-1} + \Delta B)\tau_T + (M^{-1} + \Delta C)\tau_D$. The formula can be written as:

$$\dot{V} = -M^{-1}DV + M^{-1}\tau_T + F \tag{18}$$

In (18), $F = \Delta AV + \Delta B\tau_T + (M^{-1} + \Delta C)\tau_D$, and it represents the total uncertainties of the system. In practical control, the uncertainties and disturbances are usually unknown. Therefore, it is difficult to determine the upper bound of the total uncertainties F [29]–[31]. An adaptive method can be used to estimate the total uncertainties F.

Ship position signal were set $\eta_d = [x_d, y_d, \psi_d]^T$, The adaptive sliding mode controller is designed according to the following steps:

Step 1: The position error is:

$$z_1 = \eta - \eta_d \tag{19}$$

According to (11), and because $\eta_d = [x_d, y_d, \psi_d]^T$ is constant, so:

$$\dot{z}_1 = \dot{\eta} - \dot{\eta}_d = R(\psi)V \tag{20}$$

The stability term is defined as:

$$a_1 = c_1 z_1, \quad c_1 > 0 \tag{21}$$

The Lyapunov function is defined as:

$$V_1 = \frac{1}{2}z_1^2 \tag{22}$$

Definition:

$$z_2 = \dot{z}_1 + a_1 = R(\psi)V + a_1 \tag{23}$$

Therefore:

$$\dot{V} = z_1\dot{z}_1 = z_1(z_2 - a_1) = z_1z_2 - c_1z_1^2 \tag{24}$$

Step 2:

$$\dot{z}_2 = \ddot{z}_1 + \dot{a}_1 = R(\psi)(-M^{-1}DV + M^{-1}\tau_T + F) + \dot{R}(\psi)V + \dot{a}_1 \tag{25}$$

The Lyapunov function is defined as:

$$V_2 = V_1 + \frac{1}{2}s_2^2 \tag{26}$$

where s_2 is a switching function, the switching function is defined as:

$$s_2 = k_1z_1 + z_2, \quad k_1 > 0 \tag{27}$$

Therefore:

$$\begin{aligned} \dot{V}_2 &= \dot{V}_1 + s_2\dot{s}_2 = z_1z_2 - c_1z_1^2 + s_2\dot{s}_2 \\ &= z_1z_2 - c_1z_1^2 + s_2(k_1\dot{z}_1 + \dot{z}_2) \\ &= z_1z_2 - c_1z_1^2 + s_2(k_1(z_2 - c_1z_1) \\ &\quad + R(\psi)(-M^{-1}DV + M^{-1}\tau_T + F) + \dot{R}(\psi)V + \dot{a}_1) \end{aligned} \tag{28}$$

The designed backstepping sliding mode control law is as follows:

$$\begin{aligned} \tau_T &= MR(\psi)^{-1}(-k_1(z_2 - c_1z_1) + R(\psi)M^{-1}DV \\ &\quad - R(\psi)\bar{F}\mathrm{sgn}(s_2) - \dot{R}(\psi)V - \dot{a}_1 \\ &\quad - h(s_2 + \xi \mathrm{sgn}(s_2))), \quad h > 0,\ \xi > 0 \end{aligned} \tag{29}$$

where $\bar{F}$ represents the upper bound of the total uncertainty F. Substitute (29) into (28):

$$\begin{aligned}\dot{V}_2 &= \dot{V}_1 + s_2\dot{s}_2 = z_1z_2 - c_1z_1^2 - hs_2^2 - h\xi\,|s_2| + Fs_2 - \bar{F}\,|s_2| \\ &\le -c_1z_1^2 + z_1z_2 - hs_2^2 - h\xi\,|s_2| + |s_2|\,(|F| - \bar{F}) \\ &\le -c_1z_1^2 + z_1z_2 - hs_2^2 - h\xi\,|s_2| \end{aligned} \tag{30}$$

Because:

$$\begin{aligned} z^TQz &= [z_1 \quad z_2]\begin{bmatrix} c_1 + hk_1^2 & hk_1 - \frac{1}{2} \\ hk_1 - \frac{1}{2} & h \end{bmatrix}[z_1 \quad z_2]^T \\ &= c_1z_1^2 + hk_1^2z_1^2 + 2hk_1z_1z_2 - z_1z_2 + hz_2^2 \\ &= c_1z_1^2 - z_1z_2 + hs_2^2 \end{aligned} \tag{31}$$

So (30) can be written as:

$$\dot{V}_2 \le -z^TQz - h\xi\,|s_2| \tag{32}$$

Because:

$$|Q| = h(c_1 + hk_1^2) - (hk_1 - \frac{1}{2})^2 = h(c_1 + k_1) - \frac{1}{4} \tag{33}$$

By choosing the value of h, c_1 and k_1, $|Q| > 0$ can be made, thus ensuring that Q is a positive definite matrix, then:

$$\dot{V}_2 \le 0 \tag{34}$$

It is difficult to determine the upper bound of F, so the adaptive method is adopted. Definition of Lyapunov function is:

$$V_3 = V_2 + \frac{1}{2\gamma}\tilde{F}^2 \tag{35}$$

where $\hat{F}$ is the estimation of F, the estimation error of F is $\tilde{F} = F - \hat{F}$, and γ is a positive constant, assuming F is a slow-changing disturbance, that is to say $\dot{F} = 0$, therefore:

$$\begin{aligned}\dot{V}_3 &= \dot{V}_2 - \frac{1}{\gamma}\tilde{F}\dot{\hat{F}} \\ &= z_1z_2 - c_1z_1^2 + s_2(k_1(z_2 - c_1z_1) \\ &\quad + R(\psi)(-M^{-1}DV + M^{-1}\tau_T + F) + \dot{R}(\psi)V + \dot{a}_1) \\ &\quad - \frac{1}{\gamma}\tilde{F}\dot{\hat{F}} \\ &= z_1z_2 - c_1z_1^2 + s_2(k_1(z_2 - c_1z_1) \\ &\quad + R(\psi)(-M^{-1}DV + M^{-1}\tau_T + \hat{F}) + \dot{R}(\psi)V + \dot{a}_1) \\ &\quad - \frac{1}{\gamma}\tilde{F}(\dot{\hat{F}} - \gamma s_2) \end{aligned} \tag{36}$$

The control law of the adaptive sliding mode controller is as follows:

$$\begin{aligned}\tau_T &= MR(\psi)^{-1}(-k_1(z_2 - c_1z_1) + R(\psi)M^{-1}DV \\ &\quad - R(\psi)\hat{F} - \dot{R}(\psi)V - \dot{a}_1 - h(s_2 + \xi\,\mathrm{sgn}(s_2))), \\ &\quad h > 0, \quad \xi > 0 \end{aligned} \tag{37}$$

Design the adaptive law as follows:

$$\dot{\hat{F}} = \gamma s_2 \tag{38}$$

Substitute (37) and (38) into (36):

$$\dot{V}_3 = z_1z_2 - c_1z_1^2 - hs_2^2 - h\xi\,|s_2| \tag{39}$$

According to (31), (39) can be written as:

$$\dot{V}_3 = -z^TQz - h\xi\,|s_2| \le 0 \tag{40}$$

C. ANALYSIS OF CHATTERING PHENOMENON

Chattering is common in sliding mode control [32]. The chattering phenomenon can be reduced when the approach law satisfies the following conditions:

1) Fast approach;
2) Finite time arrival;
3) When reaching the switching line, the speed is equal to zero, namely:

$$\lim_{s\to 0}\dot{s} = 0 \tag{41}$$

According to (27), we can calculate the following result:

$$\begin{aligned}\dot{s}_2 &= k_1\dot{z}_1 + \dot{z}_2 \\ &= k_1(z_2 - c_1z_1) + R(\psi)(-M^{-1}DV + M^{-1}\tau_T + F) \\ &\quad + \dot{R}(\psi)V + \dot{a}_1 \end{aligned} \tag{42}$$

Substitute (37) into (42),

$$\dot{s}_2 = -hs_2 - p\,\mathrm{sgn}(s_2), \quad h > o,\ p > 0 \tag{43}$$

In the formula above, $p = h\xi$. $-hs_2$ is the exponent approach law. We assume $\dot{\zeta} = -h\zeta$,then the solution of this equation is:

$$\zeta = \zeta(0)e^{-ht} \tag{44}$$

In the exponential approach, the approach speed is gradually reduced from a large value to zero, which not only shortens the approach time, but also makes the speed of the moving point reaching the switching surface very small. For a simple exponential approach, it is a gradual process for the moving point to approach the switching surface, which cannot guarantee the arrival of finite time, and there is no sliding mode on the switching surface. Therefore, an equal speed approach term $-p\,\mathrm{sgn}(s_2)$ should be added, so when s_2 is close to zero, the approach speed is p, which can guarantee the arrival of finite time. In addition, according to (43), we can calculate:

$$\begin{cases} \lim\limits_{s_2\to 0^+}\dot{s}_2 = -h \\ \lim\limits_{s_2\to 0^-}\dot{s}_2 = h \end{cases} \tag{45}$$

When h is small enough, it can ensure that the switching speed is small and the distance through the switching surface is small, which also ensures that the chattering is reduced.

Therefore, through the above analysis, we can conclude that our control law is helpful to reduce the chattering phenomenon of sliding mode control.

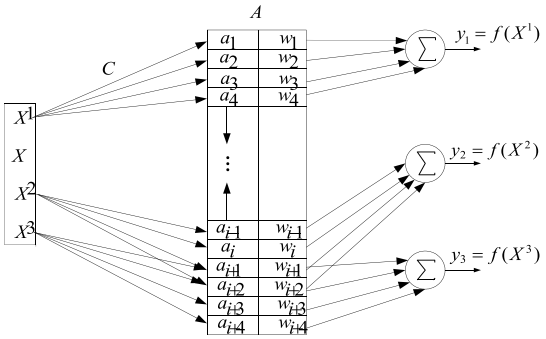

FIGURE 3. The structure of CMAC netword.

D. OPTIMAL CONTROLLER BASED ON CMAC NEURAL NETWORK

A simple CMAC structure is shown in Figure 3, where X represents the P-dimensional input state space. Let the input vector of CMAC network be represented by point $x^i = (x_1^i, x_2^i, \cdots, x_p^i)^T$ in the space X which is p-dimensional and the corresponding output vector be represented by $y_i = F(x_1^i, x_2^i, \cdots, x_p^i)$. In Figure 3, $i = 1, 2, 3$, and a point X^i in the input space will simultaneously activate N_L elements in A ($N_L = 4$ in figure 3) to make them simultaneously 1, while most other elements are 0, and the output y_i of the network is the weight summation of 4 activated units in A. It can be regarded as the receptive field size of signal detection unit. For CMAC, its working process generally includes two aspects: the calculation of results output and the generation of errors, and the adjustment of weights.

1) OUTPUT CALCULATION AND ERROR GENERATION STAGE OF CMAC

Generally speaking, each component of input vector comes from different sensors in practical application, and its value is mostly analog, while each element in A is only 0 or 1. In order to map the points in X-space to discrete points in A-space, the analog X^i must be quantized to discrete points in the input state space. Each state X^i is mapped to a set of A^i in the A-space storage area, and the N_L elements of A-space are all 1. From Figure 3, we can see that the mapping A^2 and A^3 of X^2 and X^3 in A-space appear intersection $A^2 \cap A^3$, and that means two of their corresponding four weights are the same, so the two outputs of weight accumulation and calculation are also close. From the point of view of function mapping, this feature can play a role of generalization. Obviously, for far away samples X^1 and X^3, $A^1 \cap A^3$ mapped to A-space is an empty set. This generalization does not work, so it is a local generalization. The nearer the input space is, the closer the elements in the intersection set are to N_L after mapping to A-space storage area. The intersection of the corresponding input samples in A-space plays a role in clustering the similar samples.

In order to have a unique mapping for each state of X-space in A-space, the number of cells in memory of A-space should be at least equal to the number of states in X-space, and that is $n \geq q^p$. Let each component of three-dimensional input be quantized to 10 levels, then $n \geq 1000$. For many practical systems, q^p is often much larger than this number. The mapping from A-space to A_i is Hash coding. It is a common technique for compressing sparse matrices, which is implemented by a program that generates random numbers. The address of A-space is the A_i of program generated by random number, and the random number is the address of A_i. In A_i, there are N_L random addresses corresponding to each sample. The weights stored in N_L addresses are acquired by learning, and their sum is the output of CMAC. Its expression is:

$$y_i = \sum_{j=1}^{N_L} w_j a_j(x) \quad i = 1, \cdots, m \tag{46}$$

Among them, w_j is the weight of the j memory cell. If $a_j(x)$ is activated, the value is 1. Only N_L memory cells have an effect on the output. Similar input-activated storage units overlap to produce similar outputs, and inconsistent inputs produce inconsistent outputs. The corresponding error expression is:

$$\Delta E_i = \overline{y_s} - \sum_{j=1}^{N_L} w_j a_j(x) \quad i = 1, 2, \cdots, m \tag{47}$$

2) WEIGHT ADJUSTMENT PHASE OF CMAC

In the output phase of CMAC algorithm, the actual output is generated from the CMAC storage unit. The learning process updates the weight of the CMAC storage unit according to the error between the expected output and the actual output. In conventional CMAC algorithm, errors are distributed equally to all activated storage units. Let s be a state and $w_j(t)$ be the weight stored in the j storage unit after t iteration. The conventional CMAC update $w_j(t)$ algorithm is:

$$w_j(t) = w_j(t-1) + \frac{\alpha}{N_L} a_j(\overline{y_s} - \sum_{j=1}^{N_L} a_j(x) w_j(t-1)) \tag{48}$$

$\overline{y_s}$ is the expected output of s; $\sum_{j=1}^{N_L} a_j(x) w_j(t-1)$ is the actual output of s; a is the learning constant.

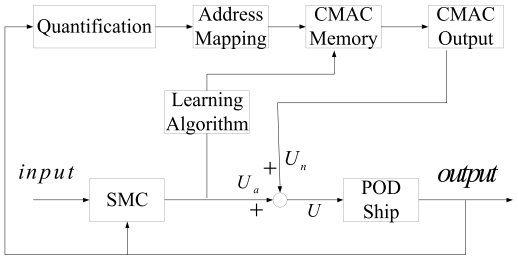

FIGURE 4. The structure of CMAC optimal controller.

The structure of CMAC optimal controller is shown in Figure 4. To sum up, CMAC optimal controller algorithm is as follows.

(1) A suitable adaptive backstepping sliding mode controller was designed.

(2) We use CMAC to approach the control algorithm in the way of online learning. When the output of CMAC can track the control algorithm completely, CMAC is used to control independently.

E. CONTROLLER WITH TRACKING DIFFERENTIATOR

In the process of using sliding mode controller, it is easy to produce large-scale control signals in the initial stage of the system, which will cause great impact on the system. Moreover, such large-scale control signals are almost impossible to produce in the actual process. Therefore, it is necessary to add a transition process to reduce the system overshoot. It is for this purpose that a tracking differentiator is added. The tracking differentiator should be installed after the input signal of the system.

The second-order tracking differentiator is:

$$\begin{cases} \dfrac{d(x_1(t))}{dt} = x_2(t) \\ \dfrac{d(x_2(t))}{dt} = R^2\left[-a_1(x_1(t)-\eta_d)^{\frac{m_1}{n_1}} - a_2(\dfrac{x_2(t)}{R})^{\frac{n_2}{m_2}}\right] \end{cases} \tag{49}$$

η_d is the input signal; x_1 and x_2 are the track signal and differential signal; $R > 0$; $a_1 > 0$; $a_2 > 0$; m_1, m_2, n_1 and n_2 are positive odd numbers.

The following is an analysis of stability. Because η_d is a constant matrix, so $\dot{\eta}_d = 0$. (49) can be transformed into:

$$\begin{cases} \dfrac{d(x_1(t)-c)}{dRt} = R^{-1}x_2(t) \\ \dfrac{d(R^{-1}x_2(t))}{dRt} = -a_1(x_1(t)-\eta_d)^{\frac{m_1}{n_1}} \\ \qquad\qquad - a_2(R^{-1}x_2(t))^{\frac{n_2}{m_2}} \end{cases} \tag{50}$$

We make $h = Rt$, $z_1(h) = x_1(t) - \eta_d$, $z_2(h) = R^{-1}x_2(t)$, so (50) can be transformed into:

$$\begin{cases} \dfrac{d(z_1(h))}{dh} = z_2(h) \\ \dfrac{d(z_2(h))}{dh} = -a_1(z_1(h))^{\frac{m_1}{n_1}} - a_2(z_2(h))^{\frac{n_2}{m_2}} \end{cases} \tag{51}$$

The Lyapunov function is defined as:

$$V(z_1(h), z_2(h)) = \frac{2n_1}{m_1+n_1}a_1 z_1^{\frac{m_1+n_1}{n_1}} + z_2^2(h) \tag{52}$$

Therefore:

$$\begin{aligned} &\frac{d(V(z_1(h), z_2(h)))}{dh} \\ &= 2a_1 z_1^{\frac{m_1}{n_1}}(h)\frac{d(z_1(h))}{dh} + 2z_2(h)\frac{d(z_2(h))}{dh} \\ &= 2a_1 z_1^{\frac{m_1}{n_1}}(h)z_2(h) + 2z_2(h)(-a_1 z_1^{\frac{m_1}{n_1}}(h) - a_2 z_2^{\frac{n_2}{m_2}}(h)) \\ &= -2a_2 z_2^{\frac{m_2+n_2}{m_2}}(h) \le 0 \end{aligned} \tag{53}$$

(53) is only equal to 0 at (0, 0). According to the Lyapunov theorem, (51) is asymptotically stable at (0, 0). That means $\lim_{h\to+\infty} z_1(h) = 0$, $\lim_{h\to+\infty} z_2(h) = 0$. So we can draw the following calculations:

$$\lim_{R\to+\infty}\int_{t_0}^{t_0+T}|x_1(t)-\eta_d|dt = \lim_{R\to+\infty}\frac{\int_{Rt_0}^{Rt_0+RT}|z_1(Rt)|dRt}{R} \tag{54}$$

TABLE 1. Ship size parameters.

Parameters	Numerical value
Length	156(m)
Beam	32.2(m)
Draft	7.5(m)
Square coefficient	0.755
Displacement	26426(t)
Prismatic coefficient	2.17

When $\int_{Rt_0}^{Rt_0+RT}|z_1(Rt)|dRt$ has an upper bound, (54) is equal to 0. If $\lim_{R\to+\infty}\int_{Rt_0}^{Rt_0+RT}|z_1(Rt)|dRt \to +\infty$, According to the L'Hopital's rule, (54) can be transformed into:

$$\begin{aligned} &\lim_{R\to+\infty}\int_{t_0}^{t_0+T}|x_1(t)-\eta_d|dt \\ &= \lim_{R\to+\infty}(|z_1(Rt_0+RT)|(t_0+T) - |z_1(Rt_0)|t_0) \end{aligned} \tag{55}$$

Because $\lim_{h\to+\infty} z_1(h) = 0$, therefore $\lim_{R\to+\infty}\int_{t_0}^{t_0+T}|x_1(t)-\eta_d|dt = 0$. It proves that the tracking differentiator can track the input signal after a period of time T.

When adding the tracking differentiator, (19) and (20) can be transformed into:

$$\begin{cases} z_1 = \eta - x_1(T) \\ z_2 = \dot{\eta} - x_2(T) \end{cases} \tag{56}$$

Because the differentiator is stable and bounded, the stability of the system can be guaranteed. This means that when time reaches T, $\dot{V}_3 < 0$ will be obtained.

IV. SIMULATION OF DYNAMIC POSITIONING SYSTEM FOR POD SHIP

A. SHIP PARAMETERS

The "Taian Kou" ship is as an example for this simulation. Its main parameters are shown in Table 1.

Parameters in M and D matrix can be calculated according to ship parameters. The calculation results are as follows:

$$M = \begin{bmatrix} 0.3418 & 0 & 0 \\ 0 & 0.3336 & 0.0007 \\ 0 & -0.0005 & 0.0228 \end{bmatrix} \tag{57}$$

$$D = \begin{bmatrix} 0.0044 & 0 & 0 \\ 0 & 0.0186 & -0.0029 \\ 0 & 0.0051 & 0.0024 \end{bmatrix} \tag{58}$$

The ship has two pod thrusters whose output power of 4700KW, as the main propeller of the ship, symmetrical installed in the stern; the others are a pair of side thruster with a power of 800KW, and they are not only a conventional lateral propeller, but also a thruster for the ship's dynamic positioning.

B. SIMULATION RESULTS ANALYSIS

We set the target position is (50m, 50m, 45°). $\lambda/L = 0.5$, $\varsigma_D = 0.05m$, and $\chi = 90°$. The current relative velocity is 1kn, and the direction is 30°. The relative

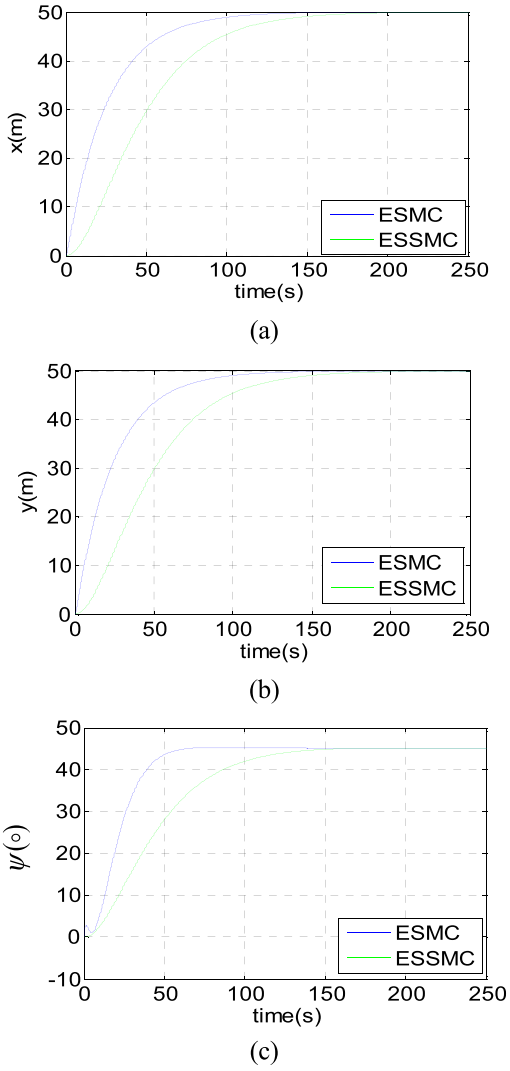

FIGURE 5. The Comparison between ESMC and ESSMC: (a) Actual position x, (b) Actual position y, (c) Heading angle.

velocity of the wind is 10kn, and the wind direction is 60°. The controller parameters are set as follows:

(1) Sliding mode control based on equal speed approach law (ESSMC): C = diag (10, 10, 30); $\varepsilon = 20$.

(2) Sliding mode control based on exponential approach law (ESMC): $\varepsilon = 20$; k = 400; $\gamma = 2$, h = 20; $c_1 = 450$; $k_1 = 50$; $\xi = 1.5$.

(3) Adaptive backstepping sliding mode control law based on CMAC neural network optimization (CSMC): $\gamma = 2$, h = 20; $c_1 = 450$; $k_1 = 50$; $\xi = 1.5$; q = 2000; C = 3; $\beta = 0.01$; $\partial = 0.1$.

(4) Controller with Tracking Differentiator (TDCSMC): $R = 200$; $a_1 = a_2 = 1$; $n_1 = n_2 = 3$; $m_1 = m_2 = 5$.

The simulation experiment is divided into three cases.

Case 1. Chattering analysis between ESSMC and ESMC.

Case 2. Comprehensive analysis of control effect between ESMC and CSMC.

Case 3. Improvement of system after adding differentiator.

Firstly, the results of case 1 are as follows:

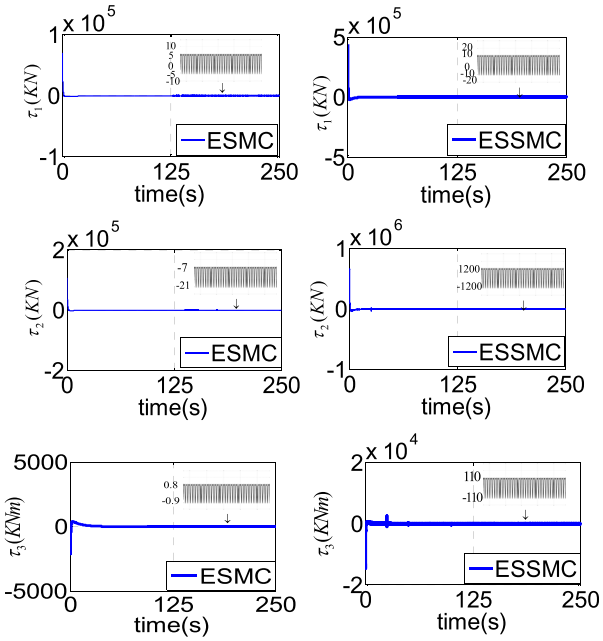

FIGURE 6. The chattering analysis between ESMC and ESSMC in transverse and longitudinal forces $\tau 1$, $\tau 2$ and moment $\tau 3$.

It can be seen from Figure 5 that both ESMC and ESSMC can meet the control requirements. ESMC greatly shortens the adjustment time, and makes the control result arrive faster.

From Figure 6, it can be seen that ESMC reduces chattering in three degrees of freedom while accelerating control time. Since the approach law of adaptive backstepping sliding mode control applied in this paper is also exponential approach, it shows that the controller designed in this paper can effectively reduce chattering.

Secondly, the dynamic positioning control results of ESMC and CSMC are compared in case 2.

From Figure 7, it can be seen that both ESMC and CSMC can achieve the goal of dynamic positioning and have good steady-state performance. But the dynamic process is different. The CSMC shortens the adjustment time and makes the unmanned surface vessel achieve its goal faster. In addition, because the dynamic positioning is at the low speed of the ship, the course change is relatively slow, so the two control laws have similar results for course control.

From Figure 8, we can see that the two control laws can make the ship's lateral speed, longitudinal speed and turning angular speed change smoothly. The CSMC control law can make the ship's speed increase faster, whether in the horizontal or vertical direction.

From Figure 9, we can see that the two controllers have calculated a stable and reliable control signal, which shows that the online learning process of cerebellar neural network is successful, and CMAC can learn sliding mode control method and maintain stability independently.

From Figure 10, F1, F2 and F3 are transverse and longitudinal forces and moment of total uncertainties. It can be seen that the estimation of uncertainties F is reasonable, bounded and convergent. The purpose of adaptive adjustment

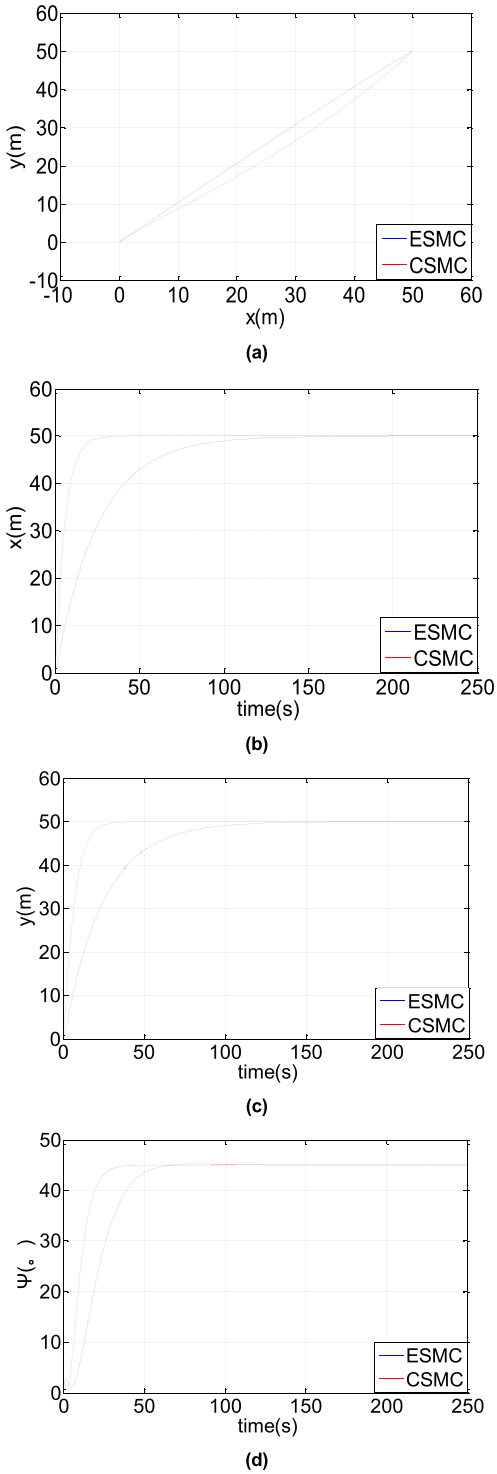

FIGURE 7. The Comparison between ESMC and CSMC: (a) Trajectory of ship in XY –plane, (b) Actual position x, (c) Actual position y, (d) Heading angle.

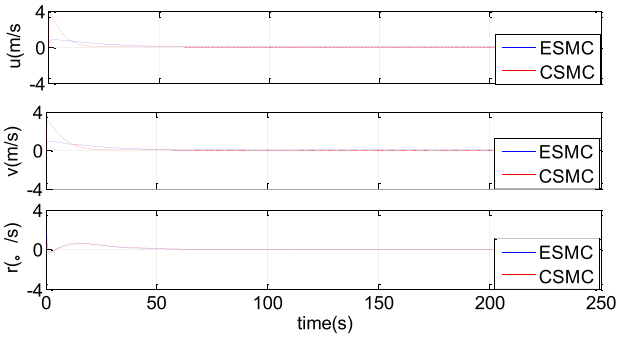

FIGURE 8. The Comparison between ESMC and CSMC in Surge Velocity u, Sway v and Yaw rate r.

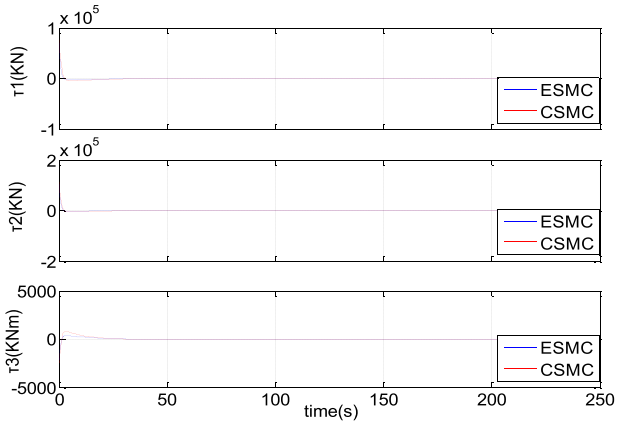

FIGURE 9. The comparison between ESMC and CSMC in transverse and longitudinal forces $\tau 1$, $\tau 2$ and moment $\tau 3$.

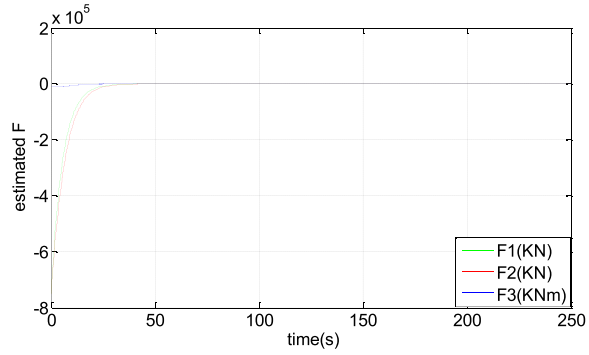

FIGURE 10. The Estimation of uncertainties F in CSMC.

controller is achieved. However, the traditional sliding mode control is prone to produce a very large control signal in the initial stage of the control process, which leads to a large estimation disturbance in the initial stage, especially in F1 and F2, resulting in a very large system oscillation in the initial stage, which is not allowed in some cases. This problem can be solved by adding tracking differentiator to arrange the transition process.

Finally, a comparative analysis of the TDCSMC and CSMC in case 3 are given.

From Figure 11, it can be seen that after adding tracking differentiator, the output of the controller is much more stable, and there will be no strong oscillation in the whole control process. This is more conducive to the practical application of the controller, and more conducive to the security of the system.

As can be seen from the comparison between Figure 12 and Figure 10, the uncertainties F is smaller and more practical than the results in Figure 10 under the same

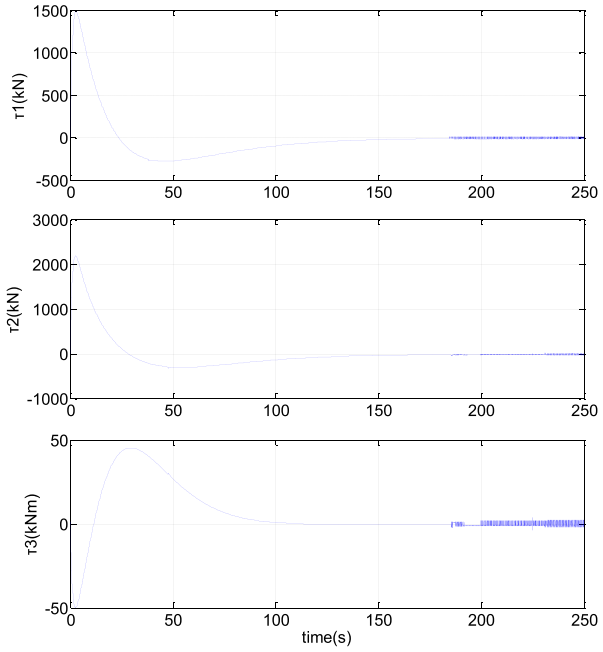

FIGURE 11. Control force $\tau 1$, $\tau 2$ and moment $\tau 3$ in TDCSMC.

TABLE 2. Performance indexes comparison of control laws.

Control laws	ESMC	CSMC	TDCSMC
Adjustment time(s)	103.5	67.5	82.7
$\overline{u}$ (m/s)	1.1	1.5	1.2
$\overline{v}$ (m/s)	0.9	1.3	1.1
$\overline{r}$ (◦ /s)	0.3	0.4	0.3
$\overline{\tau}_1$(kN)	$3.5*10^4$	$2.6*10^4$	852
$\overline{\tau}_2$ (kN)	$6.2*10^4$	$4.7*10^4$	1150
$\overline{\tau}_3$ (kNm)	220	207	51

external conditions. In particular, more reasonable estimates of F1 and F2 are given. Because the estimation of system uncertainty is more reasonable, the output of the controller does not oscillate greatly, which is more conducive to practical application. This shows the importance of arranging the transition process according to the control objective and the bearing capacity of the object, and the differential signal can be directly given by arranging the transition process through TD, which can be directly used by the controller.

Quantitative performance indexes of dynamic positioning control are shown in table 2.

In table 2, $\bar{u}$, $\bar{v}$, $\bar{r}$, $\bar{\tau}_1$, $\bar{\tau}_2$ and $\bar{\tau}_3$ indicate the average value of each quantity separately, as can be seen, the adjustment time of CSMC is less than ESMC. Because of the arrangement of transition process, the adjustment time of TDCSMC is slightly larger than CSMC, but also smaller than ESMC. $\bar{u}$, $\bar{v}$ and $\bar{r}$ in CSMC is larger than ESMC which means that the reaction speed is increased. Because the transition process slows down the reaction speed, that in TDCSMC is slightly smaller than CSMC, but also larger than ESMC. $\bar{\tau}_1$, $\bar{\tau}_2$ and $\bar{\tau}_3$

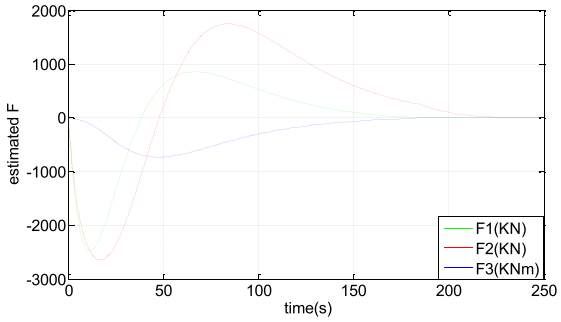

FIGURE 12. The estimation of uncertainties F in TDCSMC.

in CSMC decreases to a certain extent relative to ESMC, but it is still large in value. TDCSMC can achieve a good value. In summary, the designed control laws are proved by using Lyapunov stability theory. The control laws can control the actual position (x, y) and heading angle of the ship and remain on the expected value, and ensure that all signals in the closed-loop system of ship dynamic positioning are uniformly and eventually bounded.

V. CONCLUSION

As an important research direction of ships in the future, the dynamic positioning of unmanned surface vessel has great research value. This paper studies from the following aspects.

(1) Aiming at the dynamic positioning problem, MMG ship mathematical model is established combined with the characteristics of pod propulsion ship.

(2) A new sliding mode controller is designed based on CMAC neural network and adaptive backstepping method. The Chattering problem is analyzed in detail. In order to solve that sliding mode control is easy to generate large-scale control signals at the beginning of the control process, tracking differentiator is added to the controller.

(3) The simulation of the unmanned surface vessel's dynamic positioning system is carried out in MALAB. It can be seen from the simulation results that the designed control law has better control results than the traditional sliding mode controller. By adding tracking differentiator, the control process is smoother and the control reliability is improved.

Furthermore, this method realizes the control of the system according to the real-time information provided in the control process, which is very close to the actual engineering situation, and is welcomed by the industry, and has a broad application prospect. At the same time, its active disturbance rejection has a good prospect of improving control performance and economy. The research of this paper is expected to provide reference for the following theoretical work and engineering practice. The algorithm is universal and can solve the problem of control in the case of environmental disturbances. It can be applied in the fields of unmanned aerial vehicle (UAV) and vehicle motion control, etc.

REFERENCES

[1] J. M. Larrazabal and M. S. Peñas, "Intelligent rudder control of an unmanned surface vessel," *Expert Syst. Appl.*, vol. 55, pp. 106–117, Aug. 2016.

[2] E. Pivarčiová, P. Božek, and Y. Turygin, "Analysis of control and correction options of mobile robot trajectory by an inertial navigation system," *Int. J. Adv. Robotic Syst.*, vol. 15, no. 1, Jan. 2018, doi: 10.1177/1729881418755165.
[3] Z. Zheng, Z. Jin, L. Sun, and M. Zhu, "Adaptive sliding mode relative motion control for autonomous carrier landing of fixed-wing unmanned aerial vehicles," *IEEE Access*, vol. 5, pp. 5556–5565, 2017.
[4] J. Zheng, F. Meng, and Y. Li, "Design and experimental testing of a free-running ship motion control platform," *IEEE Access*, vol. 6, pp. 4690–4696, 2018.
[5] H. Li, P. Xie, and W. Yan, "Receding horizon formation tracking control of constrained underactuated autonomous underwater vehicles," *IEEE Trans. Ind. Electron.*, vol. 64, no. 6, pp. 5004–5013, Jun. 2017.
[6] H. Li and W. Yan, "Model predictive stabilization of constrained underactuated autonomous underwater vehicles with guaranteed feasibility and stability," *IEEE/ASME Trans. Mechatronics*, vol. 22, no. 3, pp. 1185–1194, Jun. 2017.
[7] T. I. Fossen, S. I. Sagatun, and A. J. Sørensen, "Identification of dynamically positioned ships," *Control Eng. Pract.*, vol. 4, no. 3, pp. 369–376, Mar. 1996.
[8] A. J. Sørensen, "A survey of dynamic positioning control systems," *Annu. Rev. Control*, vol. 35, no. 1, pp. 123–136, Apr. 2011.
[9] V. I. Utkin and H.-C. Chang, "Sliding mode control on electro-mechanical systems," *Math. Problems Eng.*, vol. 8, nos. 4–5, pp. 451–473, May 2002.
[10] E. A. Tannuri, A. C. Agostinho, H. M. Morishita, and L. Moratelli, "Dynamic positioning systems: An experimental analysis of sliding mode control," *Control Eng. Pract.*, vol. 18, no. 10, pp. 1121–1132, Oct. 2010.
[11] V. Utkin, "Variable structure systems with sliding modes," *IEEE Trans. Autom. Control*, vol. 22, no. AC-2, pp. 212–222, Apr. 1977.
[12] J. S. Albus, "A new approach to manipulator control: The cerebellar model articulation controller (CMAC)," *J. Dyn. Syst., Meas., Control*, vol. 97, no. 3, pp. 220–227, Sep. 1975.
[13] D. E. Thompson and S. Kwon, "Neighborhood sequential and random training techniques for CMAC," *IEEE Trans. Neural Netw.*, vol. 6, no. 1, pp. 196–202, Jan. 1995.
[14] M. Eldracher, A. Staller, and R. Pompl, "Adaptive encoding strongly improves function approximation with CMAC," *Neural Comput.*, vol. 9, no. 2, pp. 403–417, Feb. 1997.
[15] *Mathematical Model of Ship Motion: The Mechanism Modeling and Ferreting Modeling*, 1st ed. Dalian, China: Dalian Maritime University Press, 1999, pp. 294–356.
[16] H. Yasukawa and Y. Yoshimura, "Introduction of MMG standard method for ship maneuvering predictions," *J. Mar. Sci. Technol.*, vol. 20, no. 1, pp. 37–52, Mar. 2015.
[17] Z. Lei, C. Guo, and Y. Fan, "Dynamic positioning system based on active disturbance rejection technology," *J. Ocean Univ. China*, vol. 14, no. 4, pp. 636–644, Aug. 2015.
[18] A. Loria, T. I. Fossen, and E. Panteley, "A separation principle for dynamic positioning of ships: Theoretical and experimental results," *IEEE Trans. Control Syst. Technol.*, vol. 8, no. 2, pp. 332–343, Mar. 2000.
[19] E. A. Tannuri and H. M. Morishita, "Experimental and numerical evaluation of a typical dynamic positioning system," *Appl. Ocean Res.*, vol. 28, no. 2, pp. 133–146, Apr. 2006.
[20] J. Du, Y. Yang, D. Wang, and C. Guo, "A robust adaptive neural networks controller for maritime dynamic positioning system," *Neurocomputing*, vol. 110, pp. 128–136, Jun. 2013.
[21] H. Kim, H. Akimoto, and H. Islam, "Estimation of the hydrodynamic derivatives by RaNS simulation of planar motion mechanism test," *Ocean Eng.*, vol. 108, pp. 129–139, Nov. 2015.
[22] K. S. Varyani, R. McGregor, and P. Wold, "Interactive forces and moments between several ships meeting in confined waters," *Control Eng. Pract.*, vol. 6, no. 5, pp. 635–642, May 1998.
[23] H. Liang, L. Li, and J. Ou, "Fully coupled time-domain simulation of dynamic positioning semi-submersible platform using dynamic surface control," *J. Ocean Univ. China*, vol. 13, no. 3, pp. 407–414, Jun. 2014.
[24] H. Chen, T. Moan, and H. Verhoeven, "Safety of dynamic positioning operations on mobile offshore drilling units," *Rel. Eng. Syst. Saf.*, vol. 93, no. 7, pp. 1072–1090, Jul. 2008.
[25] J. K. Liu and F. C. Sun, "Research and development on sliding mode variable structure control theory and algorithm," *Control Appl.*, vol. 24, no. 3, pp. 407–418, Jun. 2007.
[26] T. Elmokadem, M. Zribi, and K. Youcef-Toumi, "Trajectory tracking sliding mode control of underactuated AUVs," *Nonlinear Dyn.*, vol. 84, no. 2, pp. 1079–1091, Apr. 2016.
[27] Q. H. Ngo and K.-S. Hong, "Sliding-mode antisway control of an offshore container crane," *IEEE/ASME Trans. Mechatronics*, vol. 17, no. 2, pp. 201–209, Apr. 2012.
[28] L. P. Perera and C. G. Soares, "Pre-filtered sliding mode control for nonlinear ship steering associated with disturbances," *Ocean Eng.*, vol. 51, pp. 49–62, Sep. 2012.
[29] Y. Liu, Y. Ma, and Y. Wang, "Reliable sliding mode finite-time control for discrete-time singular Markovian jump systems with sensor fault and randomly occurring nonlinearities," *Int. J. Robust Nonlinear Control*, vol. 28, no. 2, pp. 381–402, Jan. 2018.
[30] D. Zhao, H. Liang, and S. K. Spurgeon, "Robust adaptive terminal sliding mode control for dynamic positioning of a semi-submersible offshore platform," *Trans. Inst. Meas. Control*, vol. 41, no. 5, pp. 1361–1372, Mar. 2019.
[31] M.-R. Jeon, H.-S. Kim, J.-H. Kim, S.-J. Kim, S.-S. Song, and S.-H. Kim, "A study on the dynamic positioning control algorithm using fuzzy gain scheduling PID control theory," *J. Soc. Nav. Architects Korea*, vol. 54, no. 2, pp. 102–112, Apr. 2017.
[32] Z. Zhang, Y. Shi, Z. Zhang, and W. Yan, "New results on sliding-mode control for Takagi–Sugeno fuzzy multiagent systems," *IEEE Trans. Cybern.*, vol. 49, no. 5, pp. 1592–1604, May 2019.

ZAIJI PIAO was born in Zhalantun, China, in 1990. He received the B.S. degree in automation from Dalian Ocean University, Dalian, China, in 2013, and the M.S. degree in control engineering from Dalian Maritime University, Dalian, in 2016, where he is currently pursuing the Ph.D. degree. His research interests include ship motion control, advanced control theory, and maritime science and safety.

CHEN GUO (Member, IEEE) received the degree in automatic control from Chongqing University, in 1985, and the degree from the Dalian Institute of Marine Engineering (Automation), in 1991. He is currently a Doctoral Supervisor and the Director of the School of Ship Electrical Engineering, Institute of Ship Automation and Simulator, Dalian Maritime University. He is the Chairman of the Degree Evaluation Committee of Control Science and Engineering, the Principal of the First Level Discipline of Control Science and Engineering, and the Vice Chairman of the Academic Committee of Dalian Maritime University. He mainly engaged in marine automatic control systems, marine engine system simulation, intelligent control theory and application, and virtual reality technology and application.

SHUANG SUN was born in Zhalantun, China, in 1991. She received the B.S. degree in information management and information systems and the M.S. degree in management science and engineering from Dalian Maritime University, Dalian, China, in 2013 and 2016, respectively, where she is currently pursuing the Ph.D. degree. Her research interests include Big data processing and analysis, data mining, clustering analysis, and maritime safety.